Influence of Tip Speed Ratio on Wake Flow Characteristics Utilizing Fully Resolved CFD Methodology

Influence of Tip Speed Ratio on Wake Flow Characteristics Utilizing Fully Resolved CFD Methodology

M. Salman Siddiqui[1], Adil Rasheed[2], Trond Kvamsdal[1,2] and Mandar Tabib[2]

[1] Department of Mathematical Sciences, Norwegian University of Science and Technology, NO-7491 Trondheim, Norway
[2] SINTEF ICT, Department of Applied Mathematics, Postboks 4760 Sluppen, NO-7465 Trondheim, Norway

E-mail: muhammad.siddiqui@ntnu.no, adil.rasheed@sintef.no, trond.kvamsdal@ntnu.no, mandar.tabib@sintef.no

Abstract. Dominant flow structures in the wake region behind the turbine employed in the Blind Test campaign [1], [2] is investigated numerically. The effect on the wake configuration at variable operating conditions are studied. The importance of the introduction of turbine tower inside the numerical framework is highlighted. High-fidelity simulations are performed with Multiple Reference Frame (MRF) numerical methodology. A thorough comparison among the cases is presented, and the wake evolution is analyzed at variable stations downstream of the turbine. Streamlines of flow field traveled towards ground adjacent to turbine tower and strongly dependent on the operating tip speed ratio. Wake is composed of tower shadow superimposed by rotor wake. Shadow of the tower varies from x/R=2 until x/R=4 and breaks down into small vortices with the interaction of rotor wake. This study also shows that the wake distribution consists of two zones; inner zone composed of disturbances generated by blade root, nacelle and the tower, and an outer zone consisting of tip vortices.

1. Introduction and objective

The complex wind turbine wake dynamics, especially in the near wake, is hindering the denser layout of wind turbines inside a farm [3], [4]. It is, therefore, vital to resolve the wake to study the complex physics inside wind farms, depending on the rotor size and the blade aerodynamic characteristics. To perform such task, there are various types of methods available depending on the level of complexity to evaluate the aerodynamic behavior of wind turbines [5]. One of the most widely used analytical technique is the use of the Blade Element Momentum (BEM) theory. Experimentation, on the other hand is rigorous and complex, however, it is considered important to check the validity of numerical simulations and BEM tools [6], [7]. Due to an ever increasing size of wind turbine, it is sometimes not possible to validate the results at full scale under standard conditions [8]. Recent advancement of computers nowadays, the Computational Fluid Dynamics (CFD) is becoming a vital alternative[9]. It also offers certain advantages concerning qualitative analysis, visualizations of pressure distribution on turbine blade surfaces and evaluation of the dynamic behavior under variable inflow conditions can be

explicitly formulated [5]. It is not unique in the sense of computational cost. However, the results from the latest numerical methods give a clear depiction of flow field under real time [10], [11]. However, still, CFD methods rely on correct experimental data for the initial validation.

Therefore, to study the wake dynamics we utilized the experimental results conducted by the fellow researchers at Norwegian University of Sciences & Technology (NTNU) [12]. These experimental campaigns, known as *Blind Test*, have become popular for benchmarking and validating the performance evaluation of small wind turbines [1], [2], [13], [14], [15]. Previous studies also incorporated the effect of tower and tunnel blockage using actuator line modeling [16], [17]. To this end, we start by comparing MRF computational methodology for modeling of the flow field in wind turbines [18], [19]. Exact experimental conditions are formulated, and the ability of the present method to predict the turbine's performance under various operating conditions is evaluated. Moreover, near wake dynamics is explicitly represented with the qualitative plots of vorticity and velocity distribution in different positions in the downstream direction.

2. Governing Equations

The flow around wind turbines, even the very large ones, is still essentially incompressible with Mach numbers, hardly exceeding 0.25 based on blade tip speed. Hence, application of the incompressible form of Navier Stokes equation using a Multiple Reference Frame (MRF) is reasonably justified. Adopting the MRF approach, the computational domain is divided into two concentric zones: rotational and stationary with the former containing the rotating turbine. The governing equations are slightly modified and added with the source terms to be compatible with the reference frame in which they are solved [20]. In the stationary zone the following set

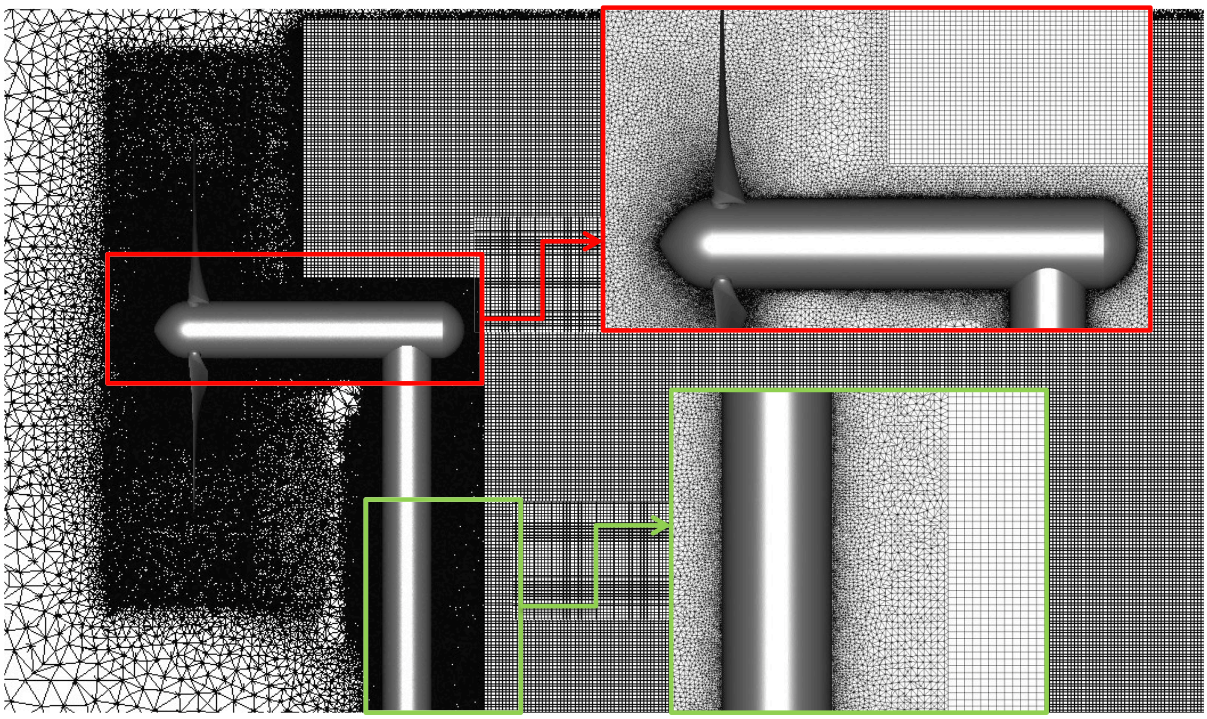

Figure 1. NTNU Blind Test T1: Computational mesh consisting of hexahedral cells in the wake block and tetrahedral cells in the rest of domain. Prism extrusion is employed to allow finer mesh grading near the turbine surface. Mesh consist of 40×10^6 elements.

of equations for mass and momentum are solved:

$$\nabla \cdot \mathbf{u_a} = 0 \tag{1}$$

$$\nabla \cdot (\mathbf{u_a} \otimes \mathbf{u_a}) = -\nabla p + \nabla \cdot (\nu + \nu_t)\nabla(\mathbf{u_a} + (\nabla \mathbf{u_a})^{\mathbf{T}}) \tag{2}$$

where $\mathbf{u_a}$ is the absolute velocity as seen from a stationary reference frame. In the rotating rotational zone the same equations are rewritten in terms of the relative speed $\mathbf{u_r}$ (relative to the rotating frame of reference) given by:

$$\nabla \cdot \mathbf{u_r} = 0 \tag{3}$$

$$\nabla \cdot (\mathbf{u_r} \otimes \mathbf{u_r}) + \mathbf{2\Omega} \times \mathbf{u_R} + \mathbf{\Omega} \times (\mathbf{\Omega} \times \mathbf{r}) = -\nabla p + \nabla \cdot (\nu + \nu_t)\nabla(\mathbf{u_r} + (\nabla \mathbf{u_r})^{\mathbf{T}}) \tag{4}$$

$$\mathbf{u_a} = \mathbf{u_r} + \mathbf{\Omega} \times \mathbf{r} \tag{5}$$

Where $\mathbf{\Omega}$ is the rotational speed of the reference frame with a stationary observer (here it will also be equal to the rotational speed of the turbine), p is pressure, ν is the kinematic viscosity of the air and ν_t is the turbulent kinetic viscosity. Since MRF computes a steady state solution, the temporal derivatives are ignored in the equations. However, the certain loss in accuracy is compensated with the substantial decrease in the solution time. The computational efficiency is considered ideal for the solution of wind turbine simulations at various operating conditions. For turbulence modeling, the $k - \omega SST$ model [21] with standard wall functions are used.

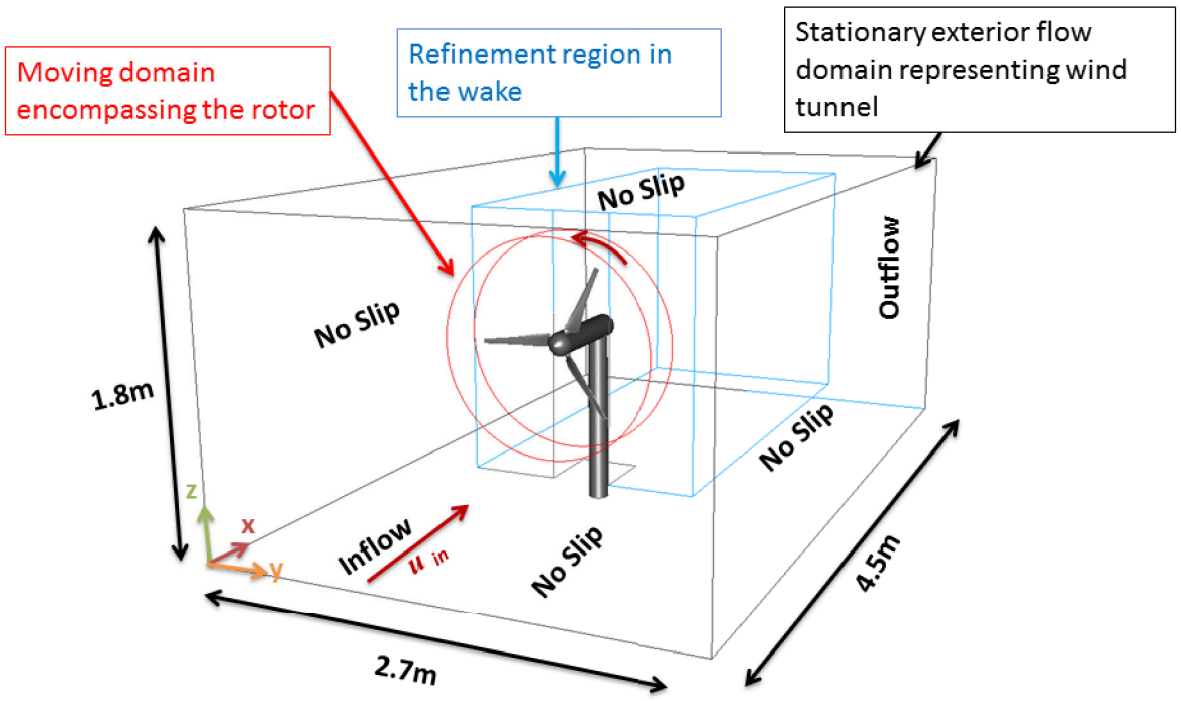

Figure 2. NTNU Blind Test T1: Computational setup and boundary conditions of full problem domain. The extent of the domain is $2.7 \times 4.5 \times 1.8$. Two zone approach is used with stationary and moving regions.

3. Approach and methods

3.1. CAD model

The geometry of the blind test turbine blade consists of 14% thick airfoil made from the standard NREL S8265MW profile with a constant twist along the spanwise direction [22]. Three such blades of 0.89m length each with very high stiffness values constitute a rotor. The high stiffness of the blades allows for neglecting the deformation in the analysis. Exact representation of experimental turbine geometry is followed; however, sharp corners in the actual geometry at the junction between blade root and nacelle are smoothened to avoid the need of excessive mesh refinements, thereby, lowering the computational cost considerably. It is assumed that such modification will not influence the analysis of wake behavior undertaken in this work. However, any modification of the sharp blade tip is avoided because of its sensitivity towards the blades aerodynamic behavior. The CAD model of the turbine is presented in Figure 1.

3.2. Domain and Mesh

A hybrid finite element mesh is generated with a smooth transition from hexahedral cells close to the blade surface to the tetrahedral elements away from it. While the former is used to model boundary layer accurately and to have better control over the y^+ (used according to the standard wall function $y^+ \approx 30$), the latter is employed because of the associated convenience towards local refinements (Figure 1). To capture the wake evolution with better accuracy, a wake block is generated with highly refined structured elements from x/R=1.5 until x/R=7. This way an accurate representation of near wake can be evaluated with an overall mesh size of around 40 $\times 10^6$ cells. The generated grid resolution is approximately two times higher than the most refined test case submitted in Blind Test campaign (CMR Prototech 26 $\times 10^6$ [1]). To construct the computational setup, we have adopted a two zones approach: stationary zone (4.5m$\times$2.7m$\times$1.8m) representing the wind tunnel and rotating region encompassing the turbine rotor. The relative tolerance between the zone is kept low (≈ 0.0001) to allow for accurate flux transfer. The computational domain is presented in Figure 2

3.3. Boundary Conditions

Simulations are conducted for uniform inlet velocity profile, applied on the inlet face and for different Tip Speed Ratio ($TSR = R\omega/U_{inf}$). The TSR is changed by adjusting the rotational speed of the turbine. At the outlet face, a standard outlet boundary condition is employed. The coupling between the rotating and stationary zone is distinguished with an interface. The walls of the wind tunnel along with the turbine surface is applied with the no-slip boundary condition, where the wall functions are employed to work with relatively coarse mesh [23]. Figure 2 represents the boundary conditions used on different faces of the computational domain, which are chosen based on the boundary conditions imposed in the experimental setup [2], [14], [22].

3.4. Computational setup and Solver

The computational setup is based on the experimental investigation described in [2][22]. Fluid parameters are selected to comply with standard operating conditions with the reference fluid density $\rho = 1.225 kg/m^3$, dynamic viscosity $\mu = 1.82 \times 10^{-5} kg/m.s$, and incoming wind velocity $U_\infty = 10 m/s$ and under varying turbine rotational speed $\Omega(rad/s) = 67, 134, 233$, which corresponds to the TSR of 3, 6, 10 respectively. The parameters of turbulent kinetic energy (k) and rate of dissipation (ω) are varied until the desired representation of turbulent intensity at the turbine location is achieved [7]. The solver is created in OpenFOAM-2.3.0 (OF) [20]. To ensure continuity, OF uses an elliptic equation for the modified pressure which involves combining the continuity equation with the divergence of the momentum equation. This elliptic equation along with the momentum equation and turbulence equation are solved in a segregated manner using the Semi-Implicit Method for Pressure-Linked Equations (SIMPLE) algorithm. The OF uses a

finite volume discretization technique, and all the equations are integrated over control volumes (CV) using Green-Gauss divergence theorem [4]. The Gauss divergence theorem converts the volume integral of the divergence of a variable into a surface integral oft the (normal component for vector valued) variable over faces comprising the CV. Thus, the divergence term defining the convection terms can simply be computed using the face values of variables in the CV. The face values of variables are obtained from their neighboring cell centered values by using convective scheme. In this work, all the equations (except k and turbulence equations) use second order linear discretization scheme, while the turbulent equations use upwind convection schemes. Similarly, the diffusion term involving Laplacian operator (the divergence of the gradient) is simplified to compute the gradient of the variable at the faces. The gradient term can be split into the contribution from the orthogonal and the non-orthogonal parts, and both these contributions are accounted for. The computations are performed on 48 cores on a 3.2 GHz Intel(R) Xeon (R) CPU machine and achieved convergence in approximately 1.5 weeks for each tip speed.

4. Result and Discussion results

4.1. Validation study

Validation against the experiment is performed to check the credibility of the simulation methodology. For the comparison of wake deficit profiles, data along the horizontal and vertical lines behind the turbine center at a location of $z = -0.95m$ to $z = +0.95m$ are extracted. Wake deficit profiles (U = 1 - U_{wake}/U_{ref}) shown in Figure 3 corresponds to a TSR=6. Hence we may infer that we have achieved a closer agreement between the given experimental data and numerical computed results. The better agreement obtained in the current investigation can be attributed to the inclusion of the nacelle and the tower in the simulation. Most of the previous studies did not include the nacelle and the tower due to computational complexity. On the other hand the MRF methodology used herein ignores the physics associated with the unsteadiness in the flow, and that can partially explain the differences between the given experimental data and the numerical simulated results. The use of the Sliding Mesh Interface (SMI) instead of MRF would enabled a better representation of the unsteadiness in the flow. The horizontal asymmetry across rotor center is successfully captured by the present simulations, the inherent reason of which is still investigated but currently unknown at present.

Having developed a sound basis through a quantitative comparison, the opportunity is

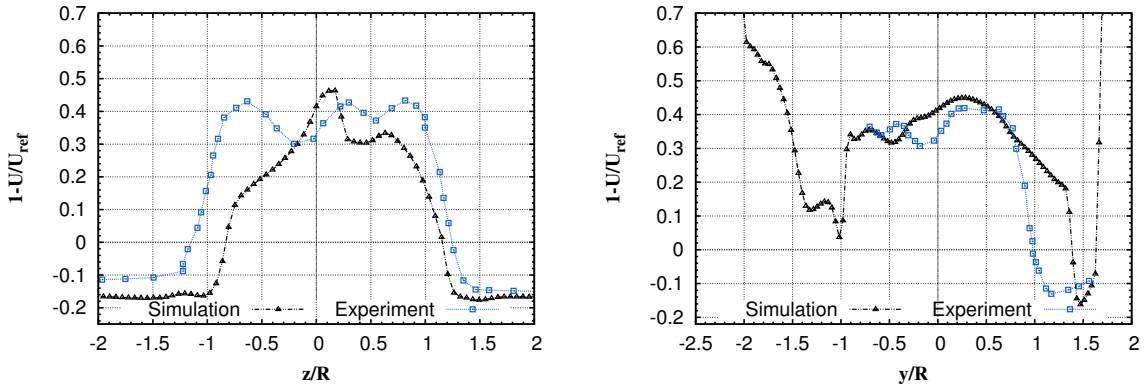

(a) Horizontal (b) Vertical

Figure 3. NTNU Blind Test T1: Validation against experimental results of Krogstad *et al.* [1] at design operating conditions of TSR=6 and at the downstream station x/R=6

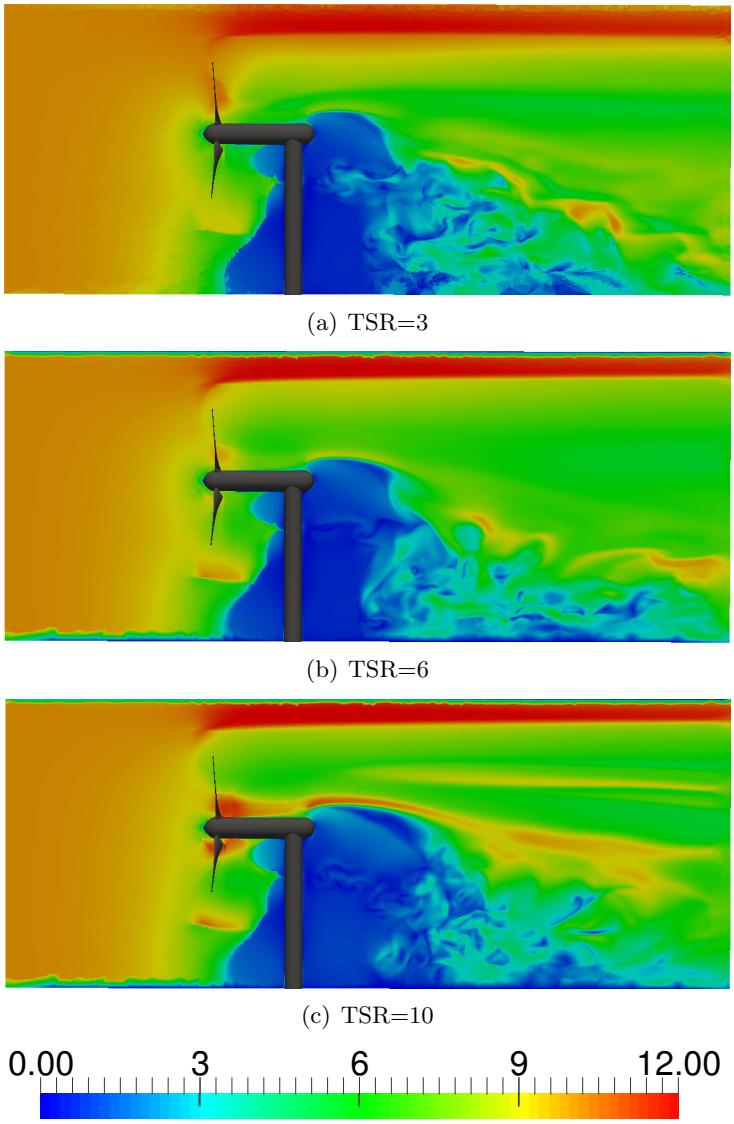

(a) TSR=3

(b) TSR=6

(c) TSR=10

Figure 4. NTNU Blind Test T1: Velocity magnitude (m/s) (inertial reference frame) at three tip speed across the turbine. Tower shadow is clearly visible along with flow acceleration at near the wind tunnel walls. Rapid flow acceleration is also observed near the hub at higher tip speeds. *units:(m/s)

exploited to evaluate the qualitative behavior of wakes at different operating conditions in the next section.

4.2. Flow dynamics versus Tip Speed Ratio (TSR)

Figure 4 presents the contour of wind speed at a 2D vertical plane passing through the center of the nacelle and aligned in the streamwise direction for the three TSRs. There are two mechanisms by which complicated flow structures are generated: One due to the movement of air around the cylindrical turbine tower including the nacelle and second due to the churning action of the rotor. These flow structures though independently generated soon interacting with each other resulting in smaller structures. This interaction causes turbulent mixing resulting in faster diffusion of the flow structures ultimately leading to full wake recovery. The restoration pattern of velocity

deficit in the presence of turbine tower, therefore, depends on the operating tip speed. Wake recovery length at $TSR = 3$ due to the presence of tower is observed to be $x/R = 4$, whereas the length increases to $x/R = 5$ at the $TSR = 10$. For the designed operating conditions of $TSR = 6$, the length lies somewhere in between the corresponding values at $TSR = 3$ and $TSR = 10$. The presence of the tower results in highly unpredictable wake behavior on the lee-side of the turbine also reported in [22].

Streamlines of velocity are found to deviate towards the ground after the interaction with the turbine structure as shown in Figure 5. This phenomenon was also reported by the authors who performed the wind tunnel experiments [2]. A similar trend is observed at each tip speed, and a complex helical streamline pattern is identified. The streamlines are found to be significantly more complex at lower TSR where the major portion of the blade is inside the stall regime [1]. On the other hand, less complicated wake structure is observed at the design TSR=6, and the streamlines are concentrated behind the turbine tower. In contrast, at TSR=10, an identical wake structure similar to TSR=3 is observed, however, the streamlines have lost their concentration and expanded indicating an increase in the overall wake width.

Constant velocity deficit is recognized in the rotor wake for the tip speed of 6. However, under off-design conditions, a significantly larger variation of flow distribution near the rotor blades is discovered. One of the interesting observation is the generation of high velocities near the turbine root at TSR of 10. It depicts that the turbine has started to work like a propeller increasing the flow velocity in the wake. Moreover, an acceleration in the flow is also observed in the streamwise direction between the rotor edge and the wind tunnel walls. The magnitude of this velocity is found to increase with the increasing tip speed. It is attributed to the blockage effect present inside the wind tunnel. This effect becomes significant at higher tip speeds where the rotor produces resistance equivalent to a solid wall to the incoming flow. Due to which a tremendous increase in the velocity between the rotor and wind tunnel walls is observed.

4.3. Formation of wake structures vs. TSR

High turbulence level pockets are generated on the lee-side of the turbine due to the presence of turbine structure as shown in Figure 6. These pockets are more significant in near wake region, where large disturbances are observed inside the wake core behind the nacelle and tower in comparison to the rotor. Wake generated from the stationary and rotating components of the turbine is distinguishable up to $x/R = 2$, where rotor shadow is separately identifiable. However, the wake starts to lose its character in the downstream direction and breaks down into

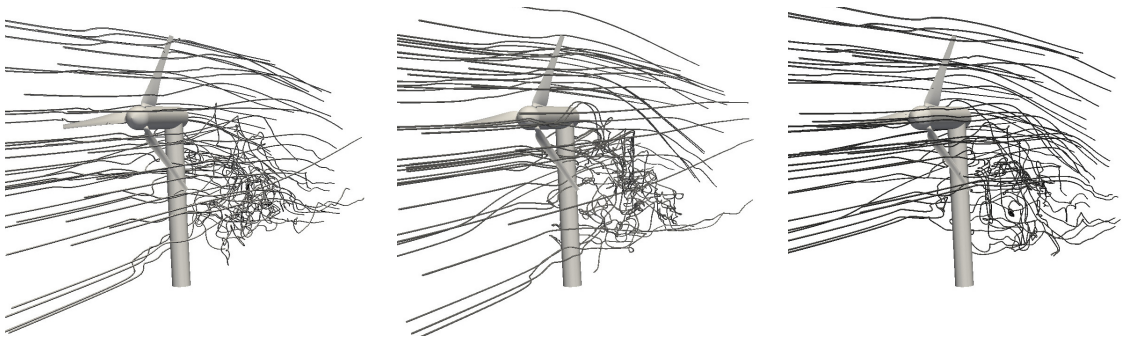

(a) TSR=3 (b) TSR=6 (c) TSRS=10

Figure 5. NTNU Blind Test T1: Streamlines of velocity along the streamwise direction (inertial reference frame) at three different tip speeds. The flow deflection towards the turbine tower is clearly visible.

smaller vortices at $x/R = 4$. Spanwise diffusion becomes active at this stage which makes the flow more homogeneous. While moving further downstream at $x/R = 6$ the difference rather becomes insignificant, and the two wakes started to diffuse together to form a combine wake.

The contours of velocity deficit recognized the asymmetry in the wake with stronger velocity reported on the left-hand side as compared to the right hand side (see Figure 6). Hence the contours also identify asymmetry in the horizontal wake profile across rotor, which is mentioned in the section 4.1. The tower wake rotates in the opposite direction to the rotor and is the prime reason for this behavior. Whereas for the off-design conditions similar lateral distribution of velocity is observed. However, the wakes overall width increases and the wake asymmetry is found to get reduced at higher TSR as compared to lower values. Moreover, the wake recovery length is examined to be considerably faster at higher tip speed as compared to smaller ones, the reason of this behavior is explained in the upcoming section.

4.4. Tower effect versus Tip Speed Ratio (TSR)

The turbine tower introduces significant variations in the flow field which enhance turbulence mixing. The distribution of fluctuations is such that intermittent spiral shape structures are

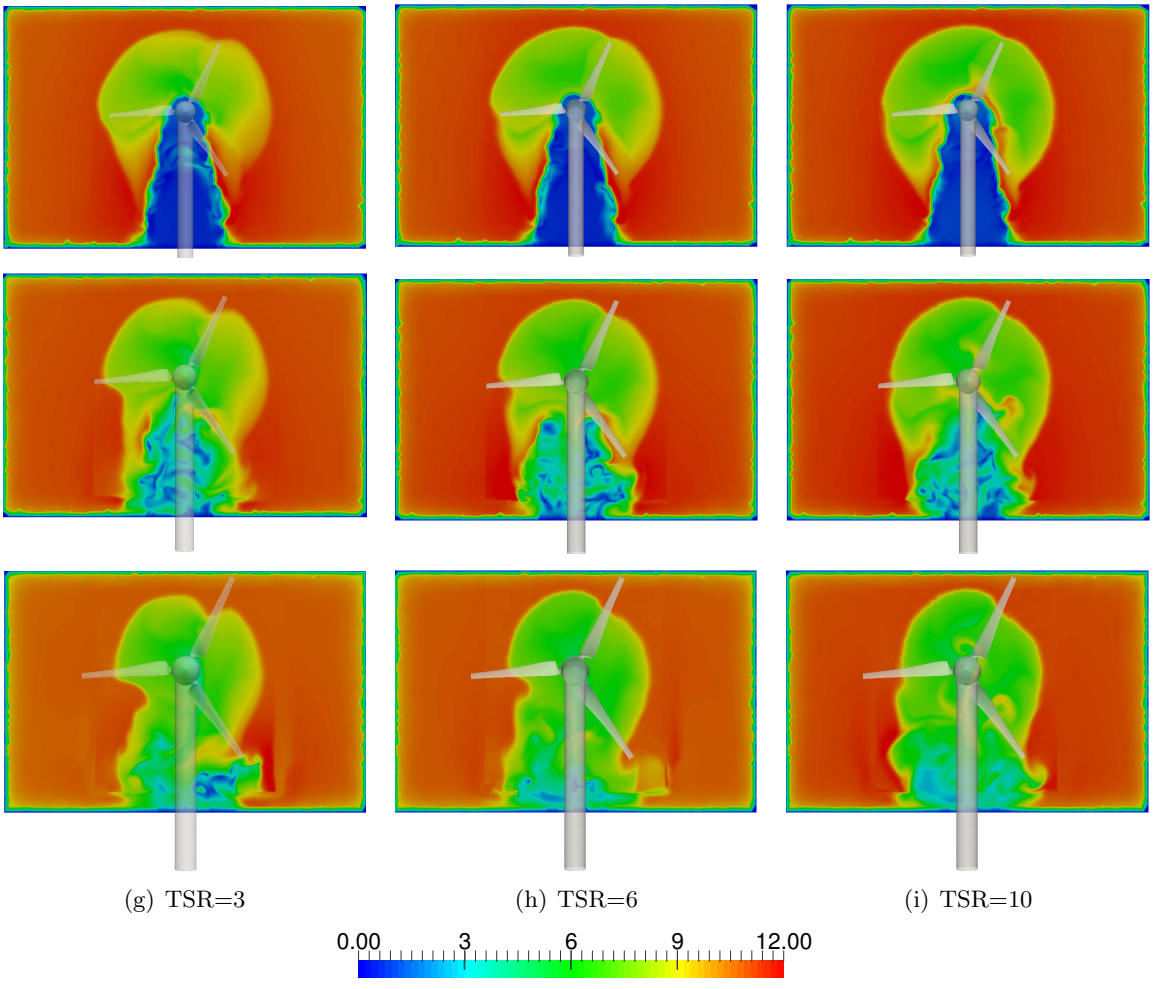

(g) TSR=3 (h) TSR=6 (i) TSR=10

Figure 6. NTNU Blind Test T1: Wake structure characterization (m/s) on x/R=2(top–row), x/R=4(intermediate–row) and x/R=6(bottom–row) at various TSR. Rotor and tower wake is clearly identified with wake expansion at higher tip speeds.

found to emerge across the cylindrical tower. It later develops into a vortex pairing in the downstream direction, where the magnitude of vorticity is found to be more behind the central region as compared to the outer region consisting of blades tip. The complex inner flow configuration is primarily composed of vortices generated by turbine root, nacelle, and the tower. The flow structures travel downwards and begin to diffuse together with the interaction and breaks into smaller vortices at x/R=3. The tip vortices, on the other hand, remains undisturbed until x/R=6, thereafter they begin to interact with the central vortex street. Overall wake profile obtained at this station have more thickness and become slightly shifted leftward from the turbine axis. It happens mainly because of the opposite directions of the tower and the rotor

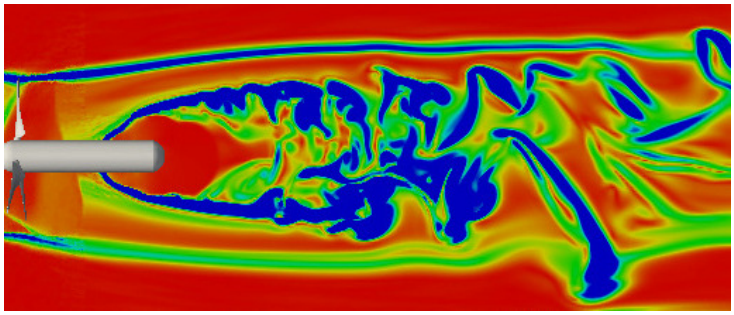

(a) TSR=3

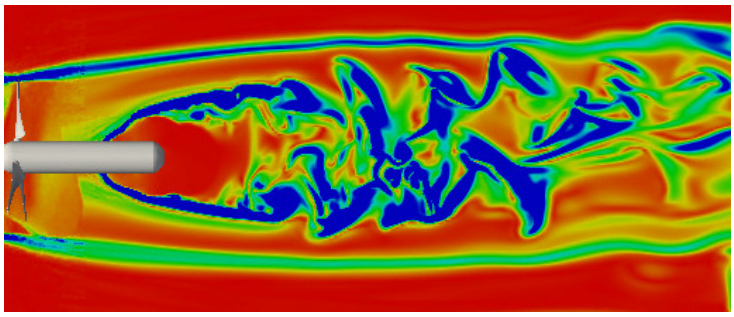

(b) TSR=6

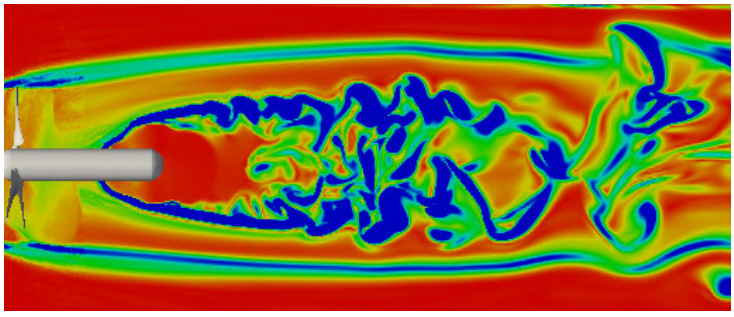

(c) TSR=10

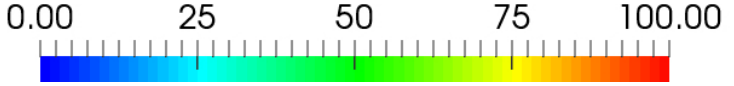

Figure 7. NTNU Blind Test T1: Vorticity (1/s) distribution from turbine tower and blade tips (inertial reference frame) at three different tip speeds. Significant vortices emanating from the turbine tip and central tower can be observed. The characteristics of wake vorticity vary with the operating tip speed.

wake.

Gradients in the flow field are lower in the central wake at x/R=6 as compared to x/R=2. This uneven distribution causes molecular diffusion and turbulent mixing which enhance wake recovery. From the Figure 7, a significant drop in the wakes strength is observed at x/R=6 for all tip speed. This region is classified as the transition zone from near wake to the complicated, far wake. Tower shadow is also recognized from the plots and is determined by a region of zero vorticity distribution near the tower. Whereas different configuration of vortices emanating from turbine structure are observed corresponding to a particular tip speed. Significantly large vortex structures are observed to originate across the cylindrical tower at lower tip speed (TSR=3). The formation evolves and break down into smaller structures while advecting downwards in the wake. However, they require more downstream distance before the fluctuations get dissipated. Whereas the vortex street at larger speed (TSR=10) results into smaller vortex structures, which disappear quick and require less distance downstream. The design condition (TSR=6) are corresponding to an average vortex pairing behavior in comparison to the off-design operating conditions.

5. CONCLUSION

Numerical investigation of wake distribution behind NTNU blind test turbine 1 was conducted under various operating conditions. Dominant components inside the near wake were identified. Reynolds Average Navier Stokes (RANS) simulations were performed with Multiple Reference Frame (MRF) methodology and k-ω SST turbulence model. The full turbine was modeled, and the boundary layer was fully resolved throughout the turbine geometry. Close agreement of mean velocity profiles in the horizontal and vertical direction was observed in the experiments. The results presented in the paper highlights the following significant observations.

- Fast recovery of velocity was observed due to the presence of turbine tower inside the computational framework. It caused an increased turbulent kinetic energy level in the wake adjacent to the turbine.
- Tower shadow comprised of region with significant higher velocity deficit. It got broken with the interaction of rotor wake and started to move towards the ground.
- Tower wake became insignificant and lost its character at x/R=6 and overall diffused wake was observed. This distance was also known as the end of near wake region.
- Vortices generated from the tower comprised of large structures at lower tip speed, where significantly smaller vortices were recognized at higher values.
- Flow streamlines followed a downward trend towards the ground at every tip speed. More concentrated streamline configurations were distinguished at lower tip speed as compared to higher values.
- Region of high velocity was recognized near blade root at higher tip speed values, which showed that turbine was enhancing flow velocity by working as a propeller.

Acknowledgments

The authors acknowledge the financial support from the Norwegian Research Council and the industrial partners of NOWITECH: Norwegian Research Centre for Offshore Wind Technology (Grant No.:193823/S60) (http://www.nowitech.no) and FSI-WT (Grant No.:216465/E20)(http://www.fsi-wt.no). Furthermore, the authors greatly acknowledge the Norwegian metacenter for computational science (NOTUR-reference number: NN9322K/1589)(www.notur.no) for giving us access to the Vilje high performance computer at the Norwegian University of Science and Technology (NTNU).

References

[1] Krogstad P A and Eriksen P E 2013 *Renewable Energy* **50** 325 – 333
[2] Krogstad P A and Saetran L 2012 *Wind Energy* **15** 443–457
[3] Siddiqui M S, Durrani N and Akhtar I 2013 *ASME Power Conference* **2** V002T09A020
[4] Cavar D, Rthor P E, Bechmann A, Sørensen N, Martinez B, Zahle F, Berg J and Kelly M 2016 *Wind Energy Science Discussions* **1** 5570
[5] Siddiqui M S, Durrani N and Akhtar I 2015 *Renewable Energy* **74** 661–670
[6] Heinz J C, Sørensen N N and Zahle F 2016 *Wind Energy* **19** 22052221 ISSN 1095-4244
[7] Siddiqui M S, Rasheed A, Kvamsdal T and Tabib M 2015 *Energy Procedia* **80** 312–320
[8] Siddiqui M S, Durrani N and Akhtar I 2013 *ASME Power Conference* **2** V002T09A020(11)
[9] Sørensen N N and Zahle F 2016 *Journal of Physics: Conference Series (Online)* **753** ISSN 1742-6596
[10] Nordanger K, Holdahl R, Kvarving A M, Rasheed A and Kvamsdal T 2015 *Computer Methods in Applied Mechanics and Engineering* **284** 664–688
[11] Nordanger K, Holdahl R, Kvamsdal T, Kvarving A M and Rasheed A 2015 *Computer Methods in Applied Mechanics and Engineering* **290** 183 – 208
[12] Eriksen P E and ge Krogstad P 2012 *Energy Procedia* **24** 378 – 384
[13] Oggiano L 2014 *Energy Procedia* **58** 111 – 116
[14] Pierella F, Krogstad P A and Saetran L 2014 *Renewable Energy* **70** 62–77
[15] Sreenivas K, Mittal A, Hereth L, Taylor L K and Hilbert C B 2016 *Journal of Wind Engineering and Industrial Aerodynamics* **157** 145 – 157
[16] Sarlak H, Nishino T, Martnez-Tossas L, Meneveau C and Sørensen J 2016 *Renewable Energy* **93** 340352
[17] Sarmast S, HSChivaee, Ivanell S and Mikkelsen R 2014 *In Journal of Physics: Conference Series* **524, No.1** 012137
[18] Siddiqui M S, Rasheed A, Tabib M and Kvamsdal T January 5-11, 2017 *35th Wind Energy Symposium AIAA SciTech Forum*
[19] Siddiqui M S, Rasheed A, Tabib M and Kvamsdal T 2016 *Journal of Physics: Conference Series* **753** 032059
[20] Jasak H 5-8 January, 2008 *47th AIAA Aerospace Sciences Meeting* **52** (AIAA 2009–341)
[21] Menter F 2009 *International Journal of Computational Fluid Dynamics* **23** 305–316
[22] Krogstad P A, Saetran L and Adaramola M S 2015 *Journal of Fluids and Structures* **52** 65–80
[23] Wilcox D 1994 *AIAA Journal. 32* 247–255